JOC Article

Theoretical Investigations on the Stereoselectivity of the Proline Catalyzed Mannich Reaction in DMSO

Waraporn Parasuk[†] and Vudhichai Parasuk*[,‡]

Department of Chemistry, Faculty of Science, Kasetsart University, Bangkok 10900, Thailand, and Department of Chemistry, Faculty of Science, Chulalongkorn University, Bangkok 10330, Thailand

fsciwapa@ku.ac.th; Vudhichai.P@chula.ac.th

Received August 22, 2008

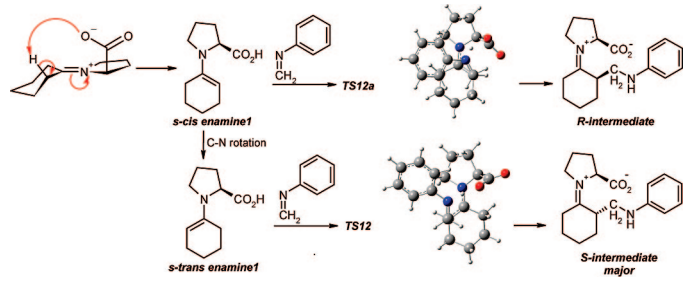

The stereocontrol steps of the (*S*)-proline catalyzed Mannich reaction of cyclohexanone, formaldehyde, and aniline were theoretically investigated. The geometries of reactants, products, and transition states were optimized using density functional theory using the B3LYP functional with the 6−31++G(d,p) basis set. The energies of these compounds were then more accurately determined at the MP2 level, and the effect of DMSO as the solvent was included using a polarizable continuum model (PCM). The reaction was modeled from the previously proposed mechanism that cyclohexanone reacts with (*S*)-proline to generate an enamine, while formaldehyde reacts with aniline to produce an imine, and that the conformation around the C−N bond of the enamine **1** is crucial for the further enantioselective step. The formation of two conformations of the enamine via a proton transfer process was examined, revealing activation barriers for *syn*- and *anti*- enamine proton transfer of 10.2 and 17.9 kcal/mol, respectively. The transformation of *syn*- to *anti*- enamine through C−N bond rotation, however, was predicted to require only 4.2 kcal/mol, while the (*S*)- and (*R*)-intermediates could be obtained from subsequent reactions between enamine and imine with energy barriers of 8.5 and 12.4 kcal/mol, respectively. The difference between these barriers, but not the C−N rotation energy, becomes larger at the MP2 level and when DMSO as a solvent is included. This predicted enantioselective reaction, through the kinetic and thermodynamic favoring of the (*S*)-pathway, is in agreement with experimental results, which have reported the (*S*)-configuration as the major product.

Introduction

The Mannich reaction is an important reaction for C−C bond formation. It is a multicomponent reaction of an aldehyde, a primary or secondary amine and a ketone. This reaction produces a Mannich base, a β-amino carbonyl compound, which is useful for the syntheses of nitrogen containing compounds, such as natural products and medicinal compounds. The stereochemistry of the Mannich base is of interest for organic chemists, and therefore, the stereoselective procedures of Mannich-type reactions have been investigated by several research groups utilizing different classes of catalysts, such as organometallic complexes, amino acids, and their derivatives.[1] Recently, the enantioselectivity and limitations of the one-pot Mannich reaction of cyclohexanone, formaldehyde, and *p*-methoxyaniline, catalyzed by (*S*)-proline and its derivatives, has been reported by Ibrahem et al.[2] The reaction is shown in Scheme 1, while the proposed mechanism of the proline catalyzed Mannich reaction is presented in Scheme 2.[3]

[†] Kasetsart University.
[‡] Chulalongkorn University.

(1) (a) List, B.; Pojarliev, P.; Biller, W. T.; Martin, H. J. *J. Am. Chem. Soc.* **2002**, *124*, 827. (b) Mitsumori, S.; Zhang, J.; Cheong, P.; Houk, H. K. N.; Tanaka, F.; Barbas, C. F., III. *J. Am. Chem. Soc.* **2006**, *128*, 1040, and references cited therein. (c) Hayashi, Y.; Urushima, T.; Aratake, S.; Okano, T.; Obi, K. *Org. Lett.* **2008**, *10*, 21, and references cited therein.

10.1021/jo801872w CCC: $40.75
Published on Web 10/28/2008

SCHEME 1. (*S*)-Proline Catalyzed One-Pot Mannich Reaction of Cyclohexanone, Formaldehyde, and *p*-Methoxyaniline

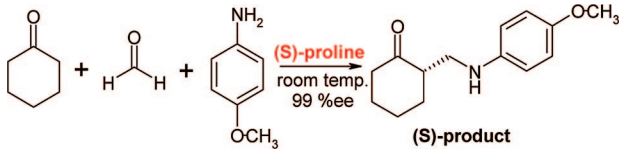

SCHEME 2. Previously Proposed Mechanism for the Proline Catalyzed Mannich Reaction[a]

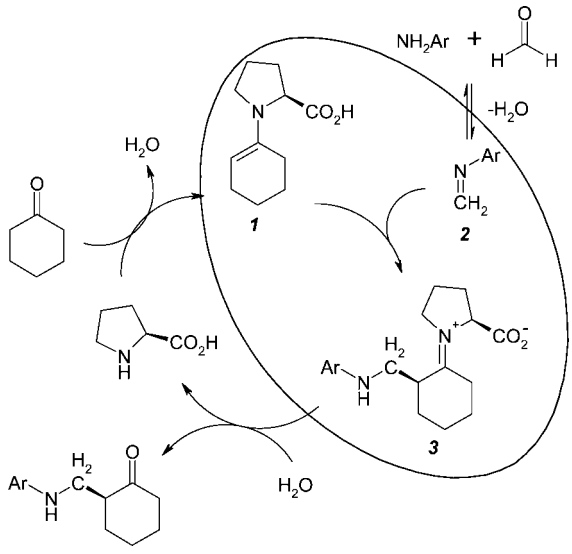

[a] The stereocontrol step is circled.

As shown in Scheme 2, proline reacts with cyclohexanone and yields enamine **1,** while formaldehyde reacts with aniline and yields imine **2**. Then, the enamine reacts with the imine to form an iminium ion intermediate **3**. A chiral center is, thus, introduced at the α-position where a new carbon−carbon bond is formed. Upon hydrolysis of the iminium ion intermediate **3**, the corresponding final product, that is, the Mannich base, is obtained. In the theoretical study of enamine formation from (*S*)-proline and acetone by density function theory using B3LYP/6−311+G(2df,p)//6−31G(d,p),[4] Boyd et al. suggested a direct proton transfer from the methyl group to the carboxylate group of the iminium zwitterion. However, the enantiomeric control step is the intermediate **3** (iminium ion) formation. Houk et al. examined possible transition state structures for the formation of iminium ions from enamine and imine also using density functional theory.[5] They found that the transition state involves hydrogen bonding between the carboxylic proton and the imine nitrogen, as shown in Figure 1. The conformation of the enamine is *anti*- and *syn*- in the transition state leading to the (*S*)- and (*R*)- intermediates, respectively. In this work, two steps of the (*S*)-proline catalyzed Mannich reaction of cyclohexanone, aniline and formaldehyde, that is, the formation of the enamine **1** and the intermediate **3**, were examined using density functional theory. Figure 2 shows the diagram for the formation steps of the enantioselective intermediate **3**. *S*- and *R*- path refer to the

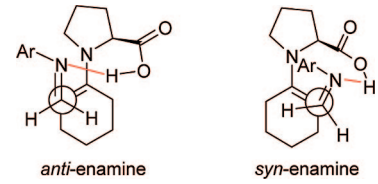

FIGURE 1. Proposed transition state of for the stereoselective step of the Mannich reaction.

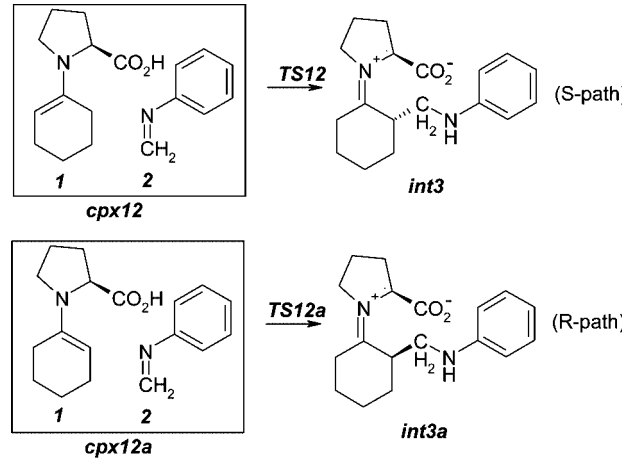

FIGURE 2. Model of the stereocontrol step.

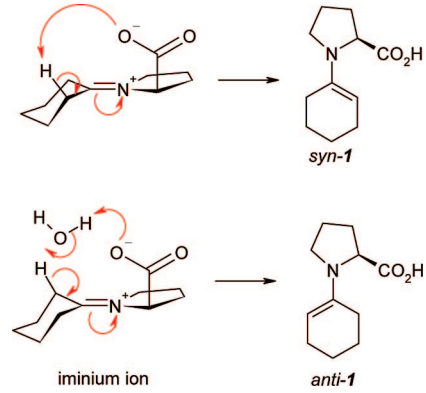

FIGURE 3. Formation of *syn*- and *anti*- enamine **1** from iminium ion via proton transfer.

reaction paths which yield the (*S*)- and (*R*)-intermediates, respectively. In the *S*- path, the *anti*- conformer of enamine **1** reacts with imine **2** through the transition state **TS12**, of which the proposed structure is displayed in Figure 1. In the *R*- path, the reactants *syn*- enamine **1** and imine **2** react through the transition state **TS12a**, also shown in Figure 1. The proton transfer process involved in the formation of both conformations around the C−N bond of enamine **1** is displayed in Figure 3. Due to the large separation, which results in a large energy barrier for the direct proton transfer process,[4] a water-assisted proton transfer was proposed for the *anti*- enamine **1**. The effect of solvent was included by using a Polarizable Continuum model (PCM) and single point MP2 calculations on the B3LYP optimized structures to more accurately determine the likely energy barriers.

Details of Calculations

Enamine 1 Formation. The proton transfer step for the formation of both conformers of enamine **1**, as shown in Figure 3,

(2) Ibrahem, I.; Zou, W.; Casas, J.; Sunden, H.; Cordova, A. *Tetrahedron* **2006**, *62*, 357.
(3) Cordova, A. *Acc. Chem. Res.* **2004**, *37*, 102.
(4) Rankin, K. N.; Gauld, J. W.; Boyd, R. S. *J. Phys. Chem. A* **2002**, *106*, 5155.
(5) Allemann, C.; Gordillo, R.; Clemente, F. R.; Cheong, P. H.; Houk, K. N. *Acc. Chem. Res.* **2004**, *37*, 558.

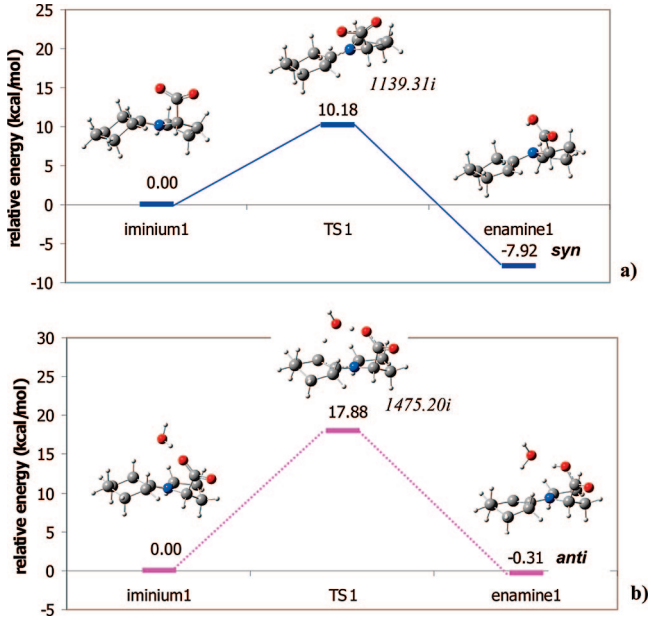

FIGURE 4. Energy profiles of the proton transfer process of (a) iminium ion to *syn*- enamine **1**, and (b) iminium ion and water to *anti*-enamine **1**.

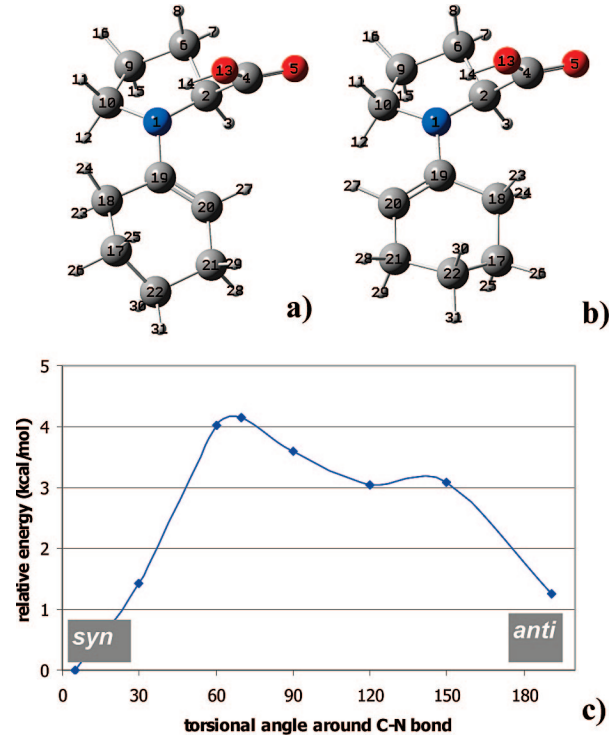

FIGURE 5. Optimized conformations of the (a) *syn*- and (b) *anti*-conformers of enamine **1**, and (c) the C19−N1 bond rotation potential energy.

was explored. The geometries of the iminium ion and enamine **1** were optimized using the B3LYP functional[6] with the 6−31++G(d,p) basis set.[7] At the same level of theory, the transition state structures of the enamine **1** formation, in both syn- and anti- conformations, were located using a QST2 approach[8] and frequency calculations were carried out to verify the transition state structures. The rotational potential around the C−N bond of enamine **1** was also examined by varying the dihedral angle C═C−N−C from 0 to 180° (*syn*- to *anti*-) using B3LYP/6−31++G(d,p). Eight selected energy points were calculated and plotted.

Intermediate 3 Formation. The kinetics of the formation of both enantiomers of intermediate **3**, that is, (*S*)-enantiomer **int3** and (*R*)-enantiomer **int3a**, from the reactant complexes of enamine **1** and imine **2**, that is, **cpx12** and **cpx12a**, were investigated. The geometries of the reactant complexes and intermediates were optimized using the B3LYP functional with the 6−31++G(d,p) basis set. The corresponding transition states, that is, **TS12** and **TS12a**, of the reactions were located using a QST2 approach[8] and frequency calculations were carried out to verify the transition state structures.

The effect of the solvent, DMSO, was evaluated using a Polarizable Continuum model (PCM)[9] with cavity modification using UFF (Universal Force Field) radii.[10] Single point MP2[11] calculations were performed at the same level of basis set on the B3LYP optimized structures. All the calculations were performed using the GAUSSIAN03 package.[12]

Results and Discussion

Since the conformation of enamine **1** is crucial for the enantiomeric formation of the intermediate **3** and then to the desired products, the formation of enamine **1** conformations was explored. This was then followed by investigation into the formation of intermediate **3**, where the stereocenter is introduced.

1. Conformations of Enamine 1. 1.1. Formation of *syn*- and *anti*- Enamine 1 via Proton Transfer. The conformation of enamine **1**, the reactant in the stereocontrol step, plays an important role in the stereochemistry of the product. Thus, the formation of *syn*- and *anti*- conformers of enamine **1** from the iminium ion via an α-proton transfer, as shown in Figure 3, was investigated. Boyd et al. reported a reaction barrier of 29.9 kcal/mol for the *syn*- enamine formation from acetone and (*S*)-proline, whereas owing to the longer distance between the α-proton and the carboxylate end the direct α-proton transfer of iminium ion to form *anti*- enamine has a ∼2.9 fold higher

(6) (a) Becke, A. D. *J. Chem. Phys.* **1993**, *98*, 5648. (b) Lee, C.; Yang, W.; Parr, R. G. *Phys. Rev. B* **1988**, *37*, 785. (c) Miehlich, B.; Savin, A.; Stoll, H.; Preuss, H. *Chem. Phys. Lett.* **1989**, *157*, 200.

(7) (a) Clark, T.; Chandrasekhar, J.; Spitznagel, G. W.; Schleyer, P. v. R. *J. Comput. Chem.* **1983**, *4*, 294. (b) Hariharan, P. C.; Pople, J. A. *Theoret. Chim. Acta* **1973**, *28*, 213. (c) Hehre, W. J.; Ditchfield, R.; Pople, J. A. *J. Chem. Phys.* **1972**, *56*, 2257.

(8) (a) Peng, C.; Schlegel, H. B. *Israel J. of Chem.* **1993**, *33*, 449. (b) Peng, C.; Ayala, P. Y.; Schlegel, H. B.; Frisch, M. J. *J. Comput. Chem.* **1996**, *17*, 49.

(9) (a) Cancès, M. T.; Mennucci, B.; Tomasi, J. *J. Chem. Phys.* **1997**, *107*, 3032. (b) Cossi, M.; Barone, V.; Mennucci, B.; Tomasi, J. *Chem. Phys. Lett.* **1998**, *286*, 253. (c) Mennucci, B.; Tomasi, J. *J. Chem. Phys.* **1997**, *106*, 5151.

(10) Rappé, A. K.; Casewit, C. J.; Colwell, K. S.; Goddard, W. A., III.; Skiff, W. M. *J. Am. Chem. Soc.* **1992**, *114*, 10024.

(11) (a) Head-Gordon, M.; Pople, J. A.; Frisch, M. J. *Chem. Phys. Lett.* **1988**, *153*, 503. (b) Frisch, M. J.; Head-Gordon, M.; Pople, J. A. *Chem. Phys. Lett.* **1990**, *166*, 275. (c) Frisch, M. J.; Head-Gordon, M.; Pople, J. A. *Chem. Phys. Lett.* **1990**, *166*, 281. (d) Head-Gordon, M.; Head-Gordon, T. *Chem. Phys. Lett.* **1994**, *220*, 122. (e) Saebo, S.; Almlof, J. *Chem. Phys. Lett.* **1989**, *154*, 83.

(12) Frisch, M. J.; Trucks, G. W.; Schlegel, H. B.; Scuseria, G. E.; Robb, M. A.; Cheeseman, J. R.; Montgomery, Jr., J. A.; Vreven, T.; Kudin, K. N.; Burant, J. C.; Millam, J. M.; Iyengar, S. S.; Tomasi, J.; Barone, V.; Mennucci, B.; Cossi, M.; Scalmani, G.; Rega, N.; Petersson, G. A.; Nakatsuji, H.; Hada, M.; Ehara, M.; Toyota, K.; Fukuda, R.; Hasegawa, J.; Ishida, M.; Nakajima, T.; Honda, Y.; Kitao, O.; Nakai, H.; Klene, M.; Li, X.; Knox, J. E.; Hratchian, H. P.; Cross, J. B.; Bakken, V.; Adamo, C.; Jaramillo, J.; Gomperts, R.; Stratmann, R. E.; Yazyev, O.; Austin, A. J.; Cammi, R.; Pomelli, C.; Ochterski, J. W.; Ayala, P. Y.; Morokuma, K.; Voth, G. A.; Salvador, P.; Dannenberg, J. J.; Zakrzewski, V. G.; Dapprich, S.; Daniels, A. D.; Strain, M. C.; Farkas, O.; Malick, D. K.; Rabuck, A. D.; Raghavachari, K.; Foresman, J. B.; Ortiz, J. V.; Cui, Q.; Baboul, A. G.; Clifford, S.; Cioslowski, J.; Stefanov, B. B.; Liu, G.; Liashenko, A.; Piskorz, P.; Komaromi, I.; Martin, R. L.; Fox, D. J.; Keith, T.; Al-Laham, M. A.; Peng, C. Y.; Nanayakkara, A.; Challacombe, M.; Gill, P. M. W.; Johnson, B.; Chen, W.; Wong, M. W.; Gonzalez, C.; and Pople, J. A. *Gaussian 03*, revision C.02; Gaussian, Inc.: Wallingford, CT, 2004.

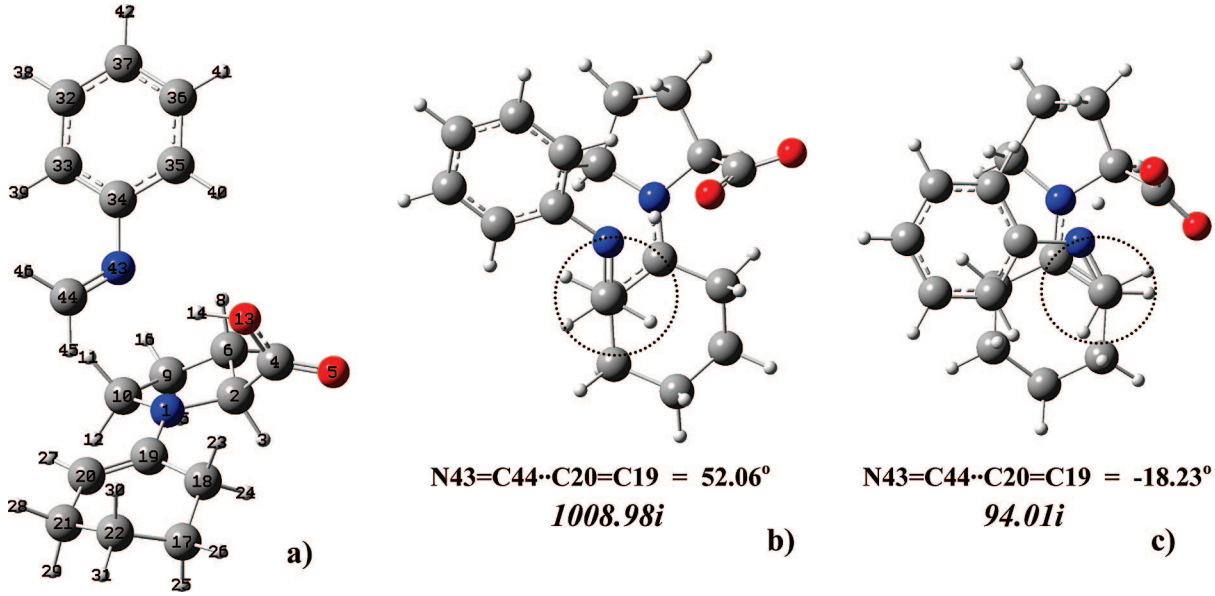

FIGURE 6. Optimized structures of (a) the reactant complex, **cpx12**, and the transition states (b) **TS12** and (c) **TS12a**.

TABLE 1. Selected Geometrical Parameters of Reactant Complexes, Transition States, and Intermediates

		distance (Å)			
	species	N43−C44	N43−H14	C20−C44	H14−O13
S- path	**Cpx12**	1.309	1.883	3.798	0.994
	TS12	1.309	1.170	2.429	1.325
	Int3	1.450	1.026	1.564	1.903
R- path	**Cpx12a**	1.308	2.104	5.146	0.985
	TS12a	1.308	1.084	2.567	1.520
	Int3a	1.438	1.022	1.590	1.958

TABLE 2. Activation Energies, E_a, of the Stereocontrol Intermediate Formation

	E_a (kcal/mol)	
method	*S*- path	*R*- path
B3LYP	8.50	12.43
DMSO	1.19	7.60
MP2	4.74	13.11

reaction barrier of 87.3 kcal/mol.[7] This suggested the formation of *anti*- enamine via the direct α-proton transfer would be most unlikely. Here, the water-assisted α-proton transfer (or indirect α-proton transfer) was proposed, as illustrated in Figure 3. The energy change along the transformation of iminium ion to enamine **1** is shown in Figure 4. The direct proton transfer of *syn*- enamine **1**, as described in Figure 3, has an activation barrier of 10.18 kcal/mol and the *syn*- enamine **1** is 7.92 kcal/mol more stable than the starting iminium ion. However, the water assisted proton transfer of *anti*- enamine **1** formation still has a significantly higher barrier, at 17.88 kcal/mol, than that for *syn*- formation, and the *anti*- enamine **1** is only 0.31 kcal/mol more stable than the iminium ion. This higher activation barrier for *anti*- enamine formation compared to that for *syn*- formation is not consistent with experimental results which found 99%ee for the (*S*)-product, suggesting the existence of an alternative pathway for *anti*- enamine **1** formation. One possible alternative is the formation of *anti*- enamine **1** via the C19−N1 bond rotation of *syn*- enamine **1** (see Figure 5).

1.2. Rotation Barrier of C19−N1 Bond. Figure 5a and b illustrate the optimized structures of the *syn*- and *anti*- conformations of enamine **1**. The optimized torsional angles C20−

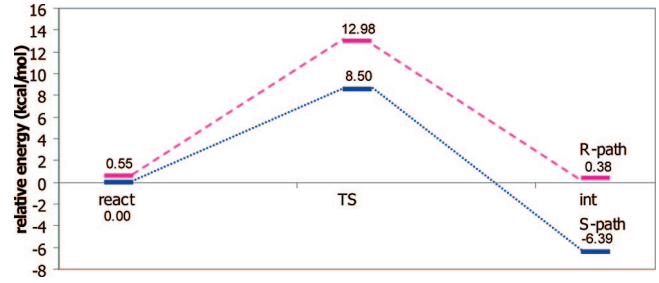

FIGURE 7. Energy profiles of the stereocontrol step and formation of intermediate **int3**, for *S*- and *R*- pathways.

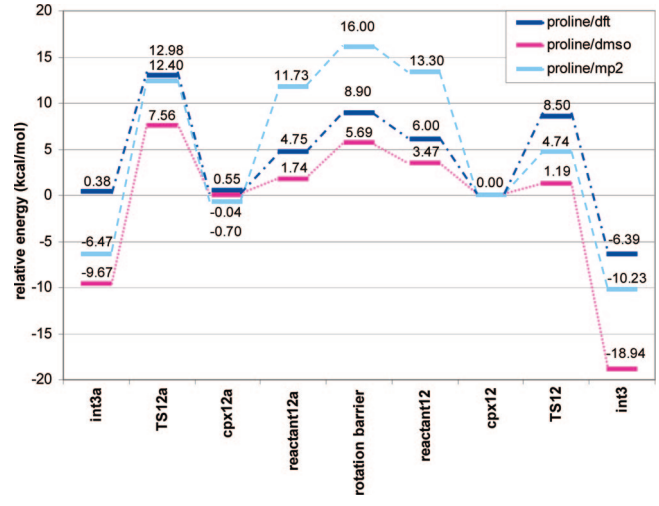

FIGURE 8. Energy profiles of the stereocontrol step of the proline catalyzed Mannich reaction evaluated with the B3LPY functional (proline/dft), and after additional MP2 calculations (proline/mp2) and inclusion of the solvent effect in DMSO (proline/dmso).

C19−N1-C2 of *syn*- and *anti*- conformers are 5.26 and 191.46°, respectively. The *syn*- conformer is 1.25 kcal/mol more stable than the *anti*- conformer. The relaxed rotation potential between *syn*- and *anti*- enamine **1** is shown in Figure 5c, with a predicted rotation barrier around the C19−N1 bond for the *syn*- to *anti*- transformation of only 4.15 kcal/mol. This barrier is much smaller than the reaction barrier of the formation of *anti*-

enamine **1** via proton transfer, as discussed in the previous subsection. Therefore, the *anti*- enamine **1**, of which the conformer is crucial for the stereoselective formation of the Mannich product, is more likely to be formed via the C−N bond rotation of the *syn*- conformer, and was further investigated.

2. Stereocontrol Step. 2.1. Geometries. Labels for the atomic positions of the reactant complexes, **cpx12** and **cpx12a**, are given in Figure 6a. These labels will be used throughout the discussion of the *S*- and *R*- intermediate pathways. The distances between the atoms directly involved in this reaction step are collected in Table 1. During the reaction progress, the acidic proton of the carboxylic group of proline, H14, is transferred to the nitrogen atom, N43, of imine **2** as the H14−O13 bond elongates from 0.994 Å in **cpx12** to 1.325 Å in **TS12** and finally 1.903 Å in **int3** and the distance N43−H14 is shortened. The double bond character between C44 and N43 of the imine **2** is also altered, as evident by the elongation of C44−N43 distance. The carbon−carbon bond formation is indicated by the shortening of C20−C44 distance of **int3**. A similar course of events is also observed for the formation of (*R*)-intermediate, **int3a**. Note that the distance C20−C44 of 5.146 Å for **cpx12a** in the *R*- path is much longer than that of 3.798 Å for **cpx12** in the *S*- path. Thus, a late transition state is expected for the *R*- path which makes the *S*- path kinetically preferred.

The geometries of the transition state for both *S*- and *R*- paths, **TS12** and **TS12a**, are shown in Figure 6b and c. The major difference between **TS12** and **TS12a** is the orientation of the atoms bonded to C20 of the enamine and C44 of the imine, which are circled in Figure 6. In **TS12**, a staggered conformation about C20 and C44 is observed, while this staggered conformation is not observed for **TS12a**, and this probably accounts for the higher energy of **TS12a**.

2.2. Energy Profile. The energies of investigated species relative to **cpx12** are schematically displayed in Figure 7. The reactant complex of the *S*- path, **cpx12**, is slightly (0.55 kcal/mol) lower in energy than the reactant complex of the *R*- path, **cpx12a**. However, the *S*- path intermediate, **int3**, is 6.77 kcal/mol more stable than *R*- path intermediate, **int3a**, and the *S*- path is 6.39 kcal/mol exothermic, in contrast to only 0.17 kcal/mol exothermic for the *R*- path reaction. Thus, the reaction through *S*- path is thermodynamically favored owing to the more stable intermediate formation. Moreover, the activation energies of the *S*- path (8.50 kcal/mol) is 3.93 kcal/mol lower than that for the *R*- path (12.43 kcal/mol). This energy difference is within the range of 2−10 kcal/mol proposed by Allemann et al.,[5] and comparable to that reported by Clemente and Houk (3.3 kcal/mol) for a stereoselective proline catalyzed aldol cyclization.[13] Thus, the *S*- path is both kinetically and thermodynamically more favorable, supporting the preference of reaction through *S*- path leading to the *S*-major product. The difference in the activation energy of 3.93 kcal/mol between the *R*- and *S*- pathways from reactant complexes corresponds to 99%ee, in agreement with the experimental findings.

3. Solvent and MP2 Calculations. Figure 8 displays the B3LYP functional and MP2 calculation derived energy profiles for the conversion of the reactant complexes, **cpx12** and **cpx12a**, to their corresponding intermediates in the gas phase, including the rotation link of the *anti*- and *syn*- enamine **1** in the reactant complexes. The B3LYP energy profile in the solvent DMSO calculated using the PCM model is also presented. At the MP2 level, the activation energy needed for the formation of **int3** from **cpx12** (4.74 kcal/mol) is smaller than that predicted by the B3LYP functional (8.50 kcal/mol), while for **int3a** formation from **cpx12a** the predicted activation energy was comparable between the MP2 and B3LYP levels but higher than that for **int3**. Inclusion of the solvent DMSO reduced the activation barrier for **int3** formation far more significantly than that for **int3a** formation, and yielded a greater exothermic reaction and more stable product. The activation energies of the reaction through the *S*- and *R*- paths are summarized in Table 2. Thus, by inclusion of the solvent effect and performing MP2 calculations, the reaction through the *S*- path is predicted to be even more preferable. That is the reaction is predicted to be more stereoselective. In contrast, they do not show any significant effect on the rotation barrier around the C−N bond of the enamine **1,** with a rotation barrier of between 4.0 to 4.2 kcal/mol being predicted for reactants **cpx12/cpx12a** by B3LYP as well as after MP2 calculations and inclusion of DMSO solvent. However, the solvent effect and MP2 calculations do shift the energies of enamine **1** significantly, being decreased and increased significantly by DMSO solvent effects and MP2 calculations, respectively, relative to that predicted by using the B3LYP functional alone.

Conclusions

In the stereocontrol step of the (*S*)-proline catalyzed Mannich reaction of cyclohexanone, formaldehyde and aniline, the formation of the *S*-intermediate, **int3**, in the *S*- path is predicted to be favored both kinetically and thermodynamically which is in agreement with previous experimentally derived data. MP2 calculations and the effect of solvent (DMSO) are predicted to further favor (*S*)-product formation, and thus a steroeselective reaction, even more. The *syn*- enamine **1** is formed directly via direct proton transfer of the iminium ion, while *anti*- enamine **1**, which is the starting conformation of the major *S*-intermediate, is formed through C−N bond rotation of *syn*- enamine **1**. MP2 calculations and the effect of solvent (DMSO) do not change the C−N bond rotation barrier.

Acknowledgment. We thank the TRF senior scholar of Thailand Research Fund, the Radchada Pisek Sompoj endowment grants of Chulalongkorn University, and the National Center of Excellence for Petroleum, Petrochemicals, and Advanced Materials, NCE-PPAM, for financial support. The Computational Chemistry Unit Cell (CCUC) of Department of Chemistry, Faculty of Science, Chulalongkorn University is acknowledged for computing facilities.

Supporting Information Available: Cartesian coordinates, total energies, and the number of imaginary frequencies for all the calculated structures. This material is available free of charge via the Internet at http://pubs.acs.org.

JO801872W

(13) Clemente, F. R.; Houk, K. N. *J. Am. Chem. Soc.* **2005**, *127*, 11294.